

Charge transfer halfcollisions: Photodissociation of the $\text{KrO}^+ 2$ cluster ion with resolution of the O_2 product vibrational states

Martin F. Jarrold, Liubomir Misev, and Michael T. Bowers

Citation: *The Journal of Chemical Physics* **81**, 4369 (1984); doi: 10.1063/1.447448

View online: <http://dx.doi.org/10.1063/1.447448>

View Table of Contents: <http://scitation.aip.org/content/aip/journal/jcp/81/10?ver=pdfcov>

Published by the **AIP Publishing**

Articles you may be interested in

[A multichannel quantum defect halfcollision analysis of \$\text{K}_2\$ photodissociation through the \$\text{B } 1\Pi\$ u state](#)
J. Chem. Phys. **95**, 4177 (1991); 10.1063/1.460773

[Erratum: Photon driven charge transfer halfcollisions: The photodissociation of \$\text{CO}_2\text{O}^+ 2\$ cluster ions with resolution of the \$\text{O}_2\$ product vibrational states \[J. Chem. Phys. 87, 2667 \(1987\)\]](#)
J. Chem. Phys. **88**, 4557 (1988); 10.1063/1.454770

[Photon driven charge transfer halfcollisions: The photodissociation of \$\text{CO}_2\text{O}^+ 2\$ cluster ions with resolution of the \$\text{O}_2\$ product vibrational states](#)
J. Chem. Phys. **87**, 2667 (1987); 10.1063/1.453105

[Halfcollision description of final state distributions of the photodissociation of polyatomic molecules](#)
J. Chem. Phys. **74**, 4380 (1981); 10.1063/1.441681

[Translational to Vibrational Energy Transfer: Impulsive Approximation for HalfCollisions](#)
J. Chem. Phys. **54**, 3652 (1971); 10.1063/1.1675400



Charge transfer half-collisions: Photodissociation of the $\text{Kr}\cdot\text{O}_2^+$ cluster ion with resolution of the O_2 product vibrational states

Martin F. Jarrold, Liubomir Misev, and Michael T. Bowers

Department of Chemistry, University of California, Santa Barbara, California 93106

(Received 23 April 1984; accepted 7 June 1984)

The photodissociation of the $\text{Kr}\cdot\text{O}_2^+$ cluster ion has been studied in the visible and UV regions of the spectrum (350–580 nm) using a crossed high energy ion beam/laser beam experiment. Photodissociation of $\text{Kr}\cdot\text{O}_2^+$ occurs by a charge transfer transition to $\text{Kr}^+\cdot\text{O}_2$ state(s). The only ionic product observed was Kr^+ . A value for the dissociation energy of the $\text{Kr}\cdot\text{O}_2^+$ cluster of $D_0^0(\text{Kr}\cdot\text{O}_2^+) \sim 0.33$ eV was estimated from the results. A compilation of ion–molecule cluster dissociation energies is given. The product angular distributions indicate that the lifetime of the excited state(s) is less than a rotational period. In the visible region of the spectrum the products are $\text{Kr}^+(^2P_{3/2}) + \text{O}_2(^2\Sigma^-)$. For the UV it is argued that one of the products is probably electronically excited [i.e., either $\text{Kr}^+(^2P_{1/2})$ or $\text{O}_2(^1\Delta_g)$]. The product relative kinetic energy distributions show resolved features that can be assigned to production of the product O_2 in specific vibrational states. Information on the product rotational excitation was also derived from these results. The potential surfaces of the $[\text{Kr}\cdot\text{O}_2]^+$ system are discussed along with literature data on the charge transfer reaction between Kr^+ and O_2 .

I. INTRODUCTION

Photodissociation is of both practical and fundamental importance. From a fundamental point of view photodissociation is interesting because it provides a field of study where the usually distinct areas of spectroscopy and molecular dynamics come together and play an intimately connected role. The first step, absorption of the photon, involves spectroscopy and the molecular dynamics comes into the subsequent dissociation. From a molecular dynamics perspective the dissociation process can be viewed as a half-collision. This concept is represented in the upper half of Fig. 1 where the dashed and solid lines together show a full collision, and the solid line represents a half-collision where optical excitation has been used to prepare the system in the middle of a collision. The advantages of using optical excitation to prepare the system are: first, that the angular momentum, and so the impact parameter, are controlled; and second, the collision geometry is defined.

The work we describe in this paper concerns charge transfer half-collisions. Referring again to the upper half of Fig. 1, the ground state is a loosely bound ion–molecule cluster $\text{A}\cdot\text{BC}^+$ and optical excitation induces charge transfer to yield an $\text{A}^+\cdot\text{BC}$ state which subsequently dissociates to yield $\text{A}^+ + \text{BC}$ products. No studies of this type have previously been reported. The specific system we discuss in this paper is $[\text{Kr}\cdot\text{O}_2]^+$. The energetics for this system are given in the lower half of Fig. 1. The value for the dissociation energy of the $\text{Kr}\cdot\text{O}_2^+$ cluster given in Fig. 1 is an estimate derived in the present work which is discussed in more detail below.

The photon driven charge transfer half-collision process shown in the upper half of Fig. 1 is closely related to the process of laser induced charge transfer¹ and is the reverse of radiative association. Laser induced charge transfer



occurs in intense optical fields and arises from photon absorption during the course of a collision. The difference between laser induced charge transfer and the process studied here is that in the present work the collision complex

$\text{A}\cdot\text{BC}^+$ has been stabilized. However, it is interesting to note that recent theoretical calculations on the laser induced charge transfer process²



predict that the transition dipole moment peaks at around 3 Å which is probably quite close to the bond length in $\text{Kr}\cdot\text{O}_2^+$.

The photodissociation process studied here is closely related to the charge transfer reaction (3):



The charge transfer reaction and photodissociation of $\text{Kr}\cdot\text{O}_2^+$ may involve the same potential energy surfaces. Fur-

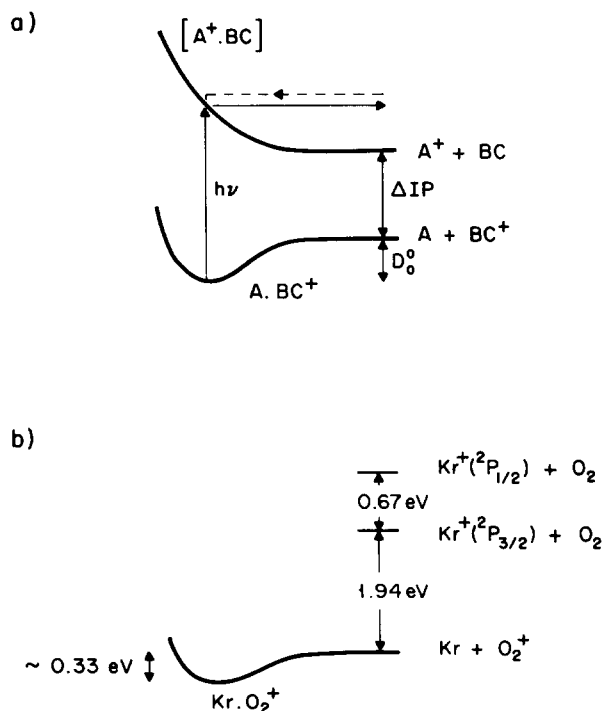


FIG. 1. Diagram showing (a) relationship between a full collision and a photon induced charge transfer half-collision, and (b) the energetics for the $[\text{Kr}\cdot\text{O}_2]^+$ system.

thermore, in the photodissociation process, once the system is prepared in the $\text{Kr}^+\cdot\text{O}_2$ state by photon absorption it is possible that instead of directly dissociating to yield $\text{Kr}^+ + \text{O}_2$ products, a "charge transfer reaction" to give $\text{O}_2^+ + \text{Kr}$ products could occur. Charge transfer [reaction (3)] is exoergic by 1.94 eV for the $^2P_{3/2}$ spin state of Kr^+ and exoergic by 2.61 eV for the $^2P_{1/2}$ spin state.³ The charge transfer reaction has been investigated by a number of workers. Adams *et al.*⁴ reported a rate constant of $4.7 \times 10^{-11} \text{ cm}^3 \text{ s}^{-1}$ (around 8% of the collision rate) for the $^2P_{3/2}$ spin state and a rate constant of $\leq 1 \times 10^{-12} \text{ cm}^3 \text{ s}^{-1}$ for the $^2P_{1/2}$ spin state. Jones *et al.*⁵ have measured the rate constants as a function of collision energy. They found that the rate constant for the $^2P_{1/2}$ state increased rapidly as the collision energy was raised but the rate constant for the $^2P_{3/2}$ state decreased.

Marx *et al.*⁶ have investigated the energy disposal in the thermal energy charge transfer reaction. Approximately 60% of the available energy is partitioned into relative kinetic energy of the products which corresponds to formation of the O_2^+ product in $v' \sim 3-4$.

We report in this paper product relative kinetic energy distributions and information on the product angular distributions for the Kr^+ product derived from the photodissociation of the $\text{Kr}\cdot\text{O}_2^+$ cluster over the wavelength range 350–580 nm. The rest of this paper is organized as follows: in the next section the experiment is briefly reviewed; this is followed by Results and Discussion sections and the paper ends with a brief Conclusion section.

II. EXPERIMENTAL

The experimental techniques have recently been described in detail elsewhere,^{7,8} consequently they will only be briefly reviewed here. A schematic diagram of the experimental apparatus is shown in Fig. 2. It consists of a reverse geometry mass spectrometer (VG Instruments, ZAB-2F), and an argon ion laser (Coherent, Innova 20) and dye laser (Coherent, model 590). Cluster ions were generated in a high

pressure ion source which was cooled to around 100 K by flowing cold nitrogen through the source block. After exiting the ion source the ions were accelerated to 8 kV and mass selected by the magnet. The mass selected ion beam then crossed the focused laser beam at the ion beam focal point in the second field free region. The photoproducts were energy analyzed by an electrostatic analyzer (ESA) using an energy resolving power of ~ 2700 FWHM, and detected using an electron multiplier. Data were accumulated using pulse counting techniques in a multichannel analyzer. The laser beam was modulated using an electronic shutter and any background product component removed by up-down counting.

The ion source was operated with an electron energy of 200–300 eV and at a total pressure of 0.11–0.13 Torr as measured with a capacitance manometer (MKS, Baratron 170M). The gas mixture employed was 0.3%–0.5% O_2 with a balance of Kr. The gases were obtained from commercial sources: O_2 from Matheson (E. D. grade) and Kr from Linde (research grade). All measurements reported here were made with the ^{84}Kr isotope.

Measurements were performed using the individual argon ion laser lines in the visible region of the spectrum, with the argon ion laser operating all lines in the UV, and with the dye laser using R6G. The output from both lasers is plane polarized with the electric vector in the vertical plane. This results in the laser polarization lying along the ion beam direction with the optics employed. For some of the experiments it was necessary to change the orientation of the laser beam polarization with respect to the ion beam direction. In the visible region of the spectrum the polarization orientation was changed using a polarization rotator (Spectra Physics). For these measurements the accuracy of the angular alignment can be checked and we estimate it to be within $\pm 1^\circ$. For the UV measurements we had to resort to changing the geometry of the optics to change the orientation of the laser polarization. In this case we estimate that the accuracy of the angular alignment is probably within $\pm 5^\circ$.

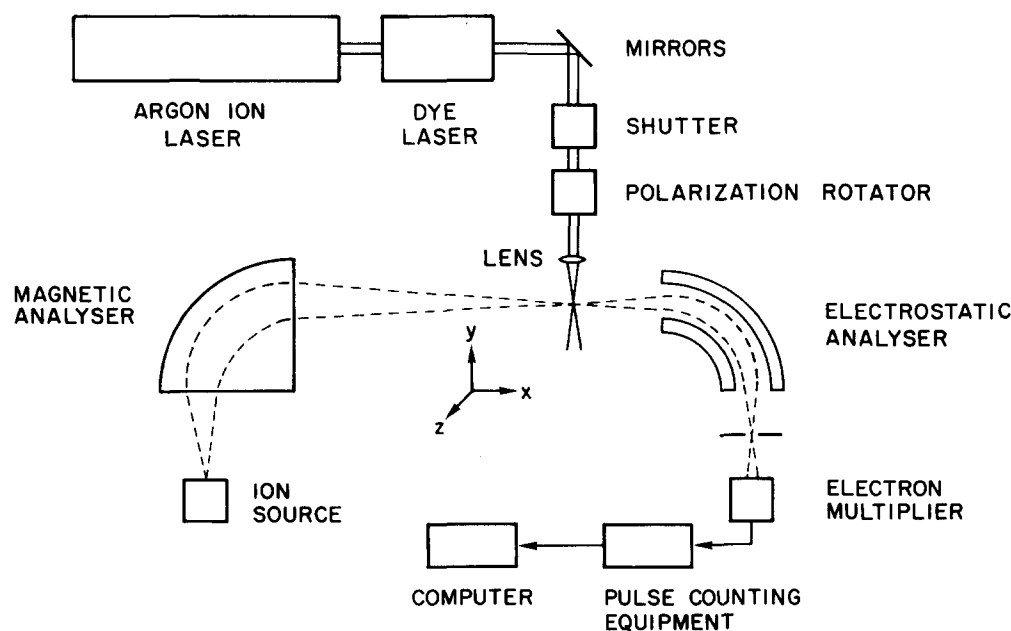


FIG. 2. Schematic diagram of the experimental apparatus.

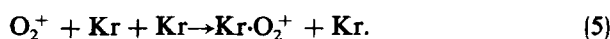
III. RESULTS

The only ionic product observed from the photodissociation of $\text{Kr}\cdot\text{O}_2^+$ was Kr^+ . No O_2^+ was observed. We estimate an upper limit on the fraction of O_2^+ produced as $< 1\%$ of the Kr^+ product. Besides $\text{O}_2^+ + \text{Kr}$ and $\text{Kr}^+ + \text{O}_2$ no other products are energetically accessible from ground state $\text{Kr}\cdot\text{O}_2^+$. The KrO^+ ion is bound by 1.2 eV^9 but formation of this ion requires breaking the strong O_2 bond.

Before proceeding to discuss our results in detail it will be useful to briefly review the ion chemistry which generates the $\text{Kr}\cdot\text{O}_2^+$ cluster in the ion source. In a mixture of 0.3%–0.5% of O_2 in Kr the primary ionization process will result in formation of Kr^+ . The Kr^+ ion will then undergo charge transfer:



Subsequently the O_2^+ will cluster with Kr :



Finally the $\text{Kr}\cdot\text{O}_2^+$ cluster may undergo a “ligand switching” reaction with O_2 :



With the small O_2 partial pressures employed the probability of a $\text{Kr}\cdot\text{O}_2^+$ cluster undergoing a ligand switching reaction before leaving the source is relatively small. However, the majority of the $\text{Kr}\cdot\text{O}_2^+$ clusters should undergo sufficient collisions with Kr , before leaving the source, to bring the clusters internal energy distribution close to a thermal distribution. We will return to the question of the $\text{Kr}\cdot\text{O}_2^+$ internal energy distribution below.

A. Product relative kinetic energy distributions

The product relative kinetic energy distributions are derived from the peaks measured with the laser polarization at the “magic angle” of 54.7° with respect to the ion beam direction.⁸ This magic angle peak is independent of the product angular distribution and only contains information about the product relative kinetic energy distribution. The product energy distribution is easily derived from the magic angle peak by taking the derivative of the peak with respect to laboratory energy and changing the energy axis to the center of mass scale.

The Kr^+/O_2 product relative kinetic energy distributions measured for the photodissociation of $\text{Kr}\cdot\text{O}_2^+$ at 514 and 458 nm are shown in Fig. 3. Several features are apparent in the distributions. In the 514 nm distribution there is a narrow peak at close to 0 eV and a peak at $\sim 0.1 \text{ eV}$. In the 458 nm distribution there are peaks at ~ 0.05 and $\sim 0.2 \text{ eV}$ and a shoulder at $\sim 0.4 \text{ eV}$. The distribution measured at 488 nm is similar to the distribution measured at 458 nm.

In order to understand the origin of the features in the kinetic energy distributions it is useful to place the distributions on a common total energy scale. This is accomplished by plotting the probabilities against the quantity $h\nu - \Delta \text{I. P.} - \text{KE}$ where $\Delta \text{I. P.}$ is given by $\text{I. P.}(\text{Kr}) - \text{I. P.}(\text{O}_2)$ and KE is the product relative kinetic energy. The resulting plot is shown in Fig. 4. Several correlations in the positions of the features in the distribution are evident. The peak in the 514

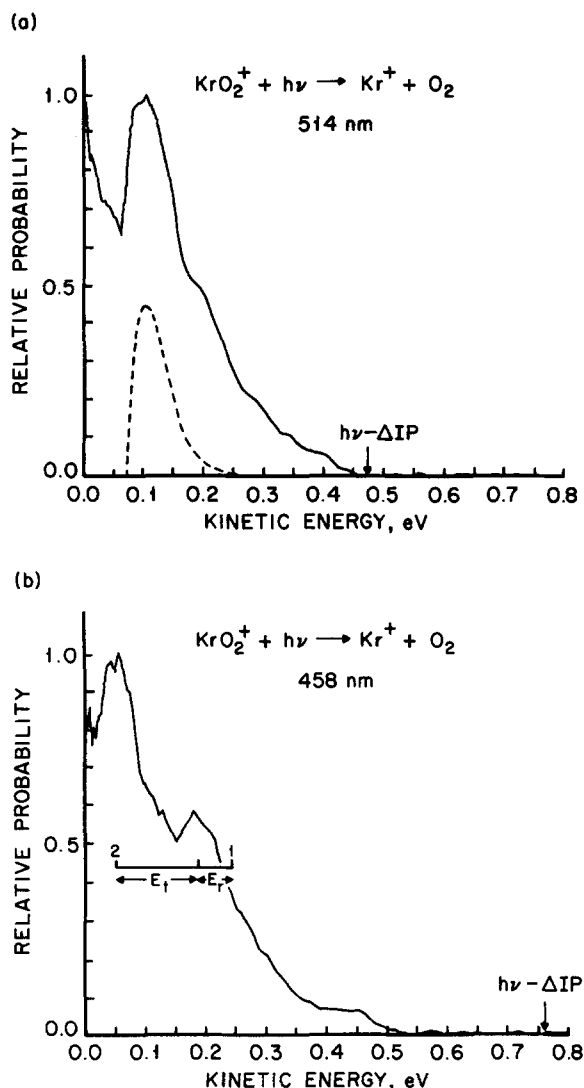


FIG. 3. Product relative kinetic energy distributions for the photodissociation of $\text{Kr}\cdot\text{O}_2^+$ to yield Kr^+ for (a) 514 nm and (b) 458 nm. The dashed line in (a) shows the calculated thermal internal energy distribution in $\text{Kr}\cdot\text{O}_2^+$ for a temperature of 100 K (see the text). Its position along the kinetic energy axis has been arbitrarily adjusted.

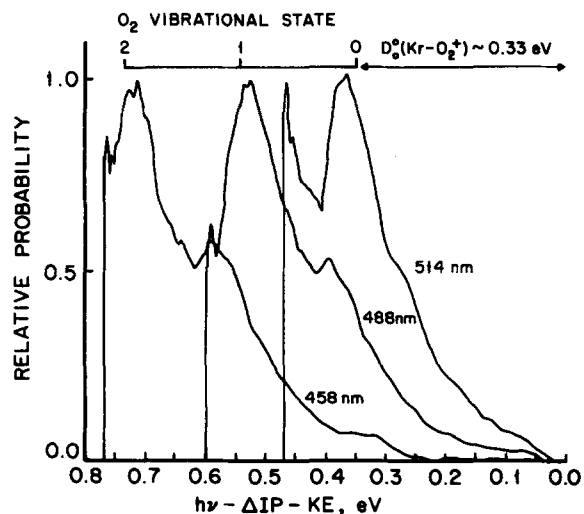


FIG. 4. Plot of the relative probability against the quantity $h\nu - \Delta \text{I. P.} - \text{KE}$ (see the text) for the photodissociation of $\text{Kr}\cdot\text{O}_2^+$ at 514, 488, and 458 nm.

nm distribution at $h\nu - \Delta I. P. - KE \sim 0.35$ eV is at approximately the same value of $h\nu - \Delta I. P. - KE$ as the smaller peak in the 488 nm distribution and the shoulder in the 458 nm distribution. Note that on going from 514 to 488 nm and then to 458 nm the feature becomes less well resolved and shifted to slightly larger values of $h\nu - \Delta I. P. - KE$. In a similar manner the sharp peak in the 514 nm distribution (at ~ 0.47 eV) can be correlated with the large peak in the 488 nm distribution located at $h\nu - \Delta I. P. - KE \sim 0.53$ eV. This peak is just beginning to "grow into" the 514 nm distribution. The smaller peak in the 458 nm distribution at $h\nu - \Delta I. P. - KE \sim 0.58$ can also be correlated with the large peak in the 488 nm distribution. Note that the peak in the 458 nm distribution is less well resolved and shifted to slightly larger values of $h\nu - \Delta I. P. - KE$. This behavior is similar to that noted for the features located near $h\nu - \Delta I. P. - KE \sim 0.35$ eV.

Conservation of energy requires

$$h\nu - \Delta I. P. - KE = D_0^\circ(\text{Kr-O}_2^+) + E_{\text{INT}}(\text{O}_2) - E_{\text{INT}}(\text{Kr-O}_2^+), \quad (7)$$

where $E_{\text{INT}}(\text{O}_2)$ is the internal (vibrational + rotational) energy of the product O_2 and $E_{\text{INT}}(\text{Kr-O}_2^+)$ is the internal energy of the Kr-O_2^+ cluster. For the time being we will ignore the initial internal energy of the Kr-O_2^+ cluster and focus on the other two terms in Eq. (7), i.e., $D_0^\circ(\text{Kr-O}_2^+) + E_{\text{INT}}(\text{O}_2)$. The dissociation energy of the cluster is not known. A scale at the top of Fig. 4 shows the spacing between the vibrational energy levels of O_2 (0.196 eV¹⁰). It is clear that the separation between the features in the distributions matches the separation between the O_2 vibrational energy levels. Thus we assign the features at ~ 0.35 eV to O_2 in the $v = 0$ state, the peaks at ~ 0.55 eV to O_2 in the $v = 1$ state and the peak at ~ 0.75 eV to O_2 in the $v = 2$ state. We can then estimate the dissociation energy of the Kr-O_2^+ cluster as ~ 0.33 eV. In making this estimate we have assumed that the vibrational state assignments are correct and that both the internal energy of the Kr-O_2^+ and the rotational excitation of the product O_2 formed in the highest accessible vibrational state are small. In fact, for the peaks corresponding to formation of O_2 in the highest accessible vibrational state the relative kinetic energy is small so the average product rotational excitation will also be small and will probably largely cancel the uncertainty due to the internal energy of the Kr-O_2^+ . Thus the estimate $D_0^\circ(\text{Kr-O}_2^+) \sim 0.33$ eV is reasonably good and is probably accurate to within ± 0.1 eV.

Given that the dissociation energy of the Kr-O_2^+ cluster is 0.33 eV, then product appearing at close to $h\nu - \Delta I. P. - KE = 0$ in Fig. 4 must arise from internally excited Kr-O_2^+ clusters. In fact, product close to $h\nu - \Delta I. P. - KE = 0$ must arise from Kr-O_2^+ clusters with internal energy just below the $\text{O}_2^+ + \text{Kr}$ dissociation threshold. Furthermore, we found that we could lower the photon energy (using the dye laser) so that the photon energy is less than $D_0^\circ(\text{Kr-O}_2^+) + \Delta I. P.$ and still observe photodissociation [to understand this it may be useful to refer to Fig. 1(a)]. An example product relative kinetic energy distribution is shown in Fig. 5 for a wavelength of 588 nm (2.108 eV). The distribution is very narrow and goes to zero at close to

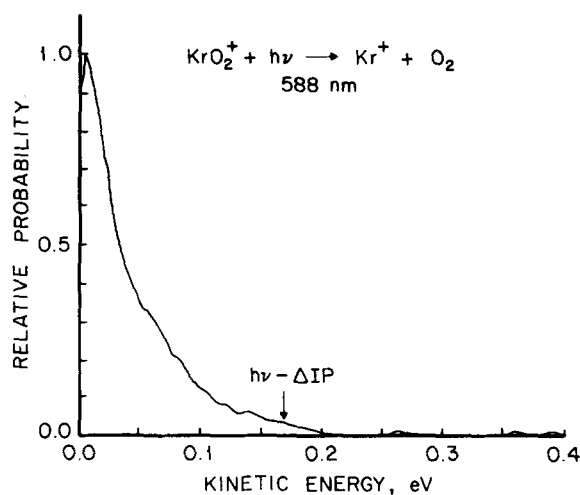


FIG. 5. Product relative kinetic energy distribution for the photodissociation of Kr-O_2^+ to yield Kr^+ at 588 nm.

$h\nu - \Delta I. P.$ The Kr^+ product observed at this wavelength must arise from Kr-O_2^+ with internal energy between 0–0.17 eV below the $\text{O}_2^+ + \text{Kr}$ dissociation threshold of Kr-O_2^+ . On lowering the photon energy further we found that the product signal decreased and, as one might expect, approached zero as the photon energy approached $\Delta I. P.$

From the preceding discussion it is clear that some of the Kr-O_2^+ clusters are internally excited. Of course some internal excitation of the clusters is expected because we will have at least a thermal distribution. For a thermal distribution the probability of a particular internal (vibrational + rotational) energy E is¹¹

$$P_{V+R}(E) = e^{-E/kT} \sum_v \eta(E_v), \quad (8)$$

where the sum is over all accessible vibrational levels up to energy E , $\eta(E_v) = 1$ for a linear molecule and $\eta(E_v) = (E - E_v)^{1/2}$ for a nonlinear molecule. A calculated thermal internal energy distribution¹² for a temperature of 100 K is shown as the dashed line in Fig. 3(a). An indication of the extent of internal excitation of the Kr-O_2^+ clusters can be obtained by comparing the calculated distribution with the shape of the $v = 0$ peak (at ~ 0.1 eV) in the kinetic energy distribution. A direct quantitative comparison between these distributions cannot be made because we do not know the extent of rotational excitation of the O_2 product. However, qualitatively we can see that the width of the kinetic energy distribution near the maximum is not substantially broader than the calculated thermal distribution but it has a high energy tail which extends to much larger energies. Thus it appears that all the Kr-O_2^+ clusters do not reach thermal equilibrium in the source. Finally, we should note that the internal energy distribution of the Kr-O_2^+ clusters in the ion beam and photodissociated Kr-O_2^+ could be different. The populations are related by the microscopic photodissociation cross sections $\sigma(E, J)$, and it is conceivable that the photodissociation cross sections increase with internal excitation. Thus the internal energy distribution of photodissociated Kr-O_2^+ sampled in the experiment could be nonthermal even though the distribution for Kr-O_2^+ clusters in the ion beam is thermal.

The product relative kinetic energy distributions measured for the photodissociation of Kr-O₂⁺ with the UV lines is shown in Fig. 6. The argon ion laser generates three lines in the UV region of the spectrum: strong lines at 351 and 364 nm and a weaker line at 334 nm. No attempt was made to resolve these lines. The overall shape of the kinetic energy distribution measured with the UV lines is not very different from the distributions measured using the visible lines (Fig. 3). Figure 7 shows a plot of the average product relative kinetic energies against photon energy. It is evident that the average kinetic energy measured using the UV lines (3.4–3.7 eV) is very similar to the averages measured using the visible lines of the argon ion laser in the range 2.4–2.7 eV. This observation is surprising because the photon energy for the UV lines is around 1 eV larger than for the visible lines. However, with the UV lines the higher energy Kr⁺(²P_{1/2}) spin state is accessible. The first excited O₂(¹Δ_g) state is quite low in energy (0.98 eV above the ground state¹⁰) and is also accessible from the ground state of the Kr-O₂⁺ cluster with the UV lines. Production of either Kr⁺(²P_{1/2}) or O₂(¹Δ_g) in the UV would provide an explanation for why the product relative kinetic energies measured in the UV and visible regions of the spectrum are similar.

B. Product angular distributions

Photon absorption preferentially occurs for molecules with their transition dipole moment along the electric vector of the laser beam. This anisotropic distribution generated by photoexcitation will be reflected in the product angular distribution. The product angular distribution contains information on the lifetime of the excited electronic state and on the direction of the transition dipole moment in the cluster. In our experiment the electrostatic analyzer measures the component of the ion energy along the ion beam direction. Thus if the product angular distribution is anisotropic the peak shapes measured with the laser polarization at 0° and 90° with respect to the ion beam direction will be different.

More quantitative information on the product angular distributions can be obtained by comparing the measured

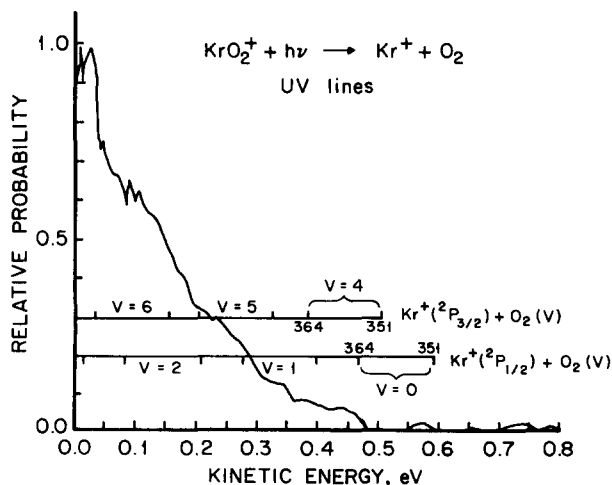


FIG. 6. Product relative kinetic energy distribution for the photodissociation of Kr-O₂⁺ to yield Kr⁺ with the UV lines (364, 351, and 334 nm).

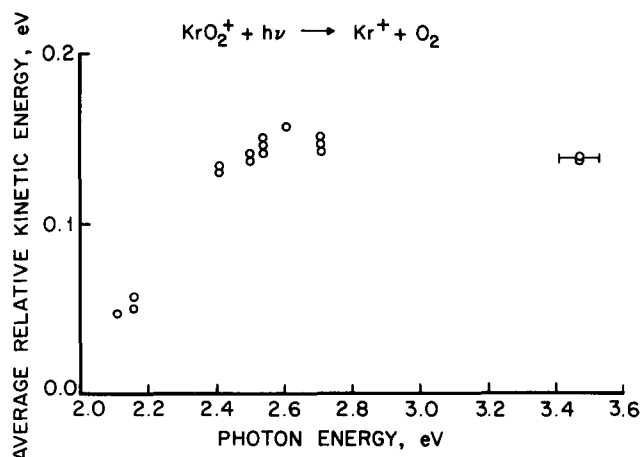


FIG. 7. Plot of the average product relative kinetic energy against photon energy for the photodissociation of Kr-O₂⁺ to yield Kr⁺.

peak shapes with a computer simulation. The methods employed have been described in detail elsewhere.⁷ The simulation employs the product relative kinetic energy distribution and the photoproducts angular distribution given by¹³

$$P(\theta) = (4\pi)^{-1} [1 + \beta P_2(\cos \theta)]. \quad (9)$$

In this equation θ is the angle between the electric vector of the laser and the axis of recoil of the Kr⁺/O₂ fragments, $P_2(\cos \theta)$ is the second degree Legendre polynomial in $\cos \theta$, and β is the asymmetry parameter. Since the product relative kinetic energies are relatively small, and comparable with the initial rotational energy of the cluster, it is necessary to take into account the deflection of the trajectory of the recoiling fragments by the rotation of the cluster. Previously we have developed a simple model to account for this effect.⁷ We assume that the deflection angle is given impulsively by

$$\alpha = \sin^{-1}(E_r/E_t)^{1/2}, \quad (10)$$

where E_r is the initial rotational energy of the cluster and E_t is the product relative kinetic energy. Averaging over a thermal rotational energy distribution the asymmetry parameter is given by

$$\beta = \beta_0 \int d\alpha P_2(\cos \alpha) P(\alpha; E_t, T), \quad (11)$$

where $P(\alpha; E_t, T)$ is the distribution function for deflection angle α for products with kinetic energy E_t , and for a thermal rotational energy distribution characterized by a temperature T . More details of the model are given elsewhere.^{7,8,14} The parameter β_0 in Eq. (11) is adjusted to give the best match with the experimental peak shapes.

The best match values of β_0 are summarized in Table I. Except for a wavelength of 575 nm it was possible to define

TABLE I. Values of the asymmetry parameter β_0 deduced from the simulations (see the text).

Wavelength (nm)	Asymmetry parameter β_0^b
UV lines ^a	1.0
458	1.2
488	1.2
514	1.0
575	>0.4

^a 334, 351, and 364 nm.

^b Estimated accuracy ± 0.2 .

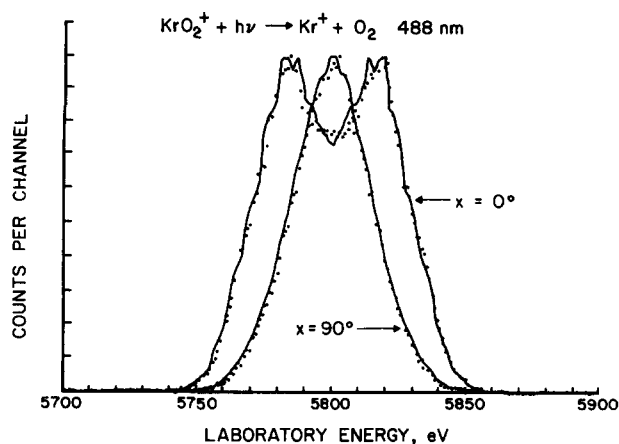


FIG. 8. Peak shapes with 0° and 90° between the laser beam polarization and the ion beam direction for the photodissociation of Kr-O₂⁺ at 488 nm. The points are the experimental data and the lines show a simulation using $\beta_0 = 1.2$ and $T = 100$ K (see the text). The small oscillations in the simulation are artifacts due to the numerical integration models used.

β_0 with a precision of ± 0.2 . For wavelengths of ≤ 514 nm β_0 has values of 1.0–1.2. An example, showing the agreement between the simulation and the experimental data, is given in Fig. 8 for a wavelength of 488 nm. The small oscillations evident in the simulation are artifacts due to the numerical

integrations. For the data measured at 575 nm it was not possible to fit the measured 0° and 90° peak shapes. As noted above, at 575 nm the photoproduct arises from internally excited Kr-O₂⁺ clusters. In addition, the product relative kinetic energies are small so it is not surprising that our simple model breaks down and fails at this wavelength. Although we were not able to accurately define the asymmetry parameter at 575 nm we were able to place a lower limit of $\beta_0 > 0.4$ on its value.

IV. DISCUSSION

The value for the dissociation energy of the Kr-O₂⁺ cluster estimated above was $D_0^\circ(\text{Kr-O}_2^+) \sim 0.33$ eV. The number of ion-molecule clusters for which dissociation energies have been measured is now fairly large. We believe that a compilation of the available data may be useful. In Table II we have summarized most of the available data for the dissociation energies of small ion-molecule clusters.^{15–53} There are two main approaches to measuring the dissociation energies: photoionization of neutral clusters and equilibrium measurements. The photoionization experiment provides a lower limit to the 0 K dissociation energy. The quantity measured in the equilibrium experiment is $-\Delta H_T^\circ$

TABLE II. Compilation of ion-molecule cluster dissociation energies.

Cluster	Dissociation energy D_0° (eV)	Method ^a	Literature reference
He-He ⁺	2.469,2.34,2.55	TC,DS,DS	15,16,17
Ne-Ne ⁺	1.36,1.35	PI,DS	18,19
Ar-Ar ⁺	1.33,1.269,1.30	PD,PI,DS	20,21,19
Kr-Kr ⁺	1.176,1.150,1.15,1.21	PD,PI,PI,DS	22,23,24,19
Xe-Xe ⁺	1.03,0.99	PI,DS	25,19
CO-CO ⁺	0.97	PI	26
N ₂ -N ₂ ⁺	1.05,(0.99), ^b 0.90	EQ,PI	27,26
O ₂ -O ₂ ⁺	0.457,0.42,0.42,0.26	EQ,PI,EQ,PI	28,29,50,51
NO-NO ⁺	0.598,0.59	PI,PI	26,30
HCl-HCl ⁺	0.87	PI	31
HBr-HBr ⁺	1.00	PI	31
H ₂ O-H ₂ O ⁺	1.58	PI	47
N ₂ O-N ₂ O ⁺	0.56	PI	32
CO ₂ -CO ₂ ⁺	0.70(0.685), ^b 0.51,0.31,0.67	EQ,PI,PI,EI	33,32,34,48
OCS-OCS ⁺	0.75	PI	35
CS ₂ -CS ₂ ⁺	0.98(0.95), ^b 0.76,0.49	EQ,PI,PI	36,37,38
SO ₂ -SO ₂ ⁺	0.66	PI	39
NH ₃ -NH ₃ ⁺	0.79	PI	40
C ₂ H ₄ -C ₂ H ₄ ⁺	0.79	PI	41
Ne-He ⁺	0.69	SP	42
Ar-Ne ⁺	0.079	PI	43
Ar-He ⁺	0.026	SP	44
Kr-Ar ⁺	0.53,0.59	PI,PI	45,46
Kr-Ne ⁺	0.055	PI	43
Xe-Kr ⁺	0.385,0.37	PI,PI	45,46
Xe-Ar ⁺	0.176,0.14	PI,PI	45,46
Xe-Ne ⁺	0.041	PI	43
Kr-O ₂ ⁺	0.33	PD	This work
Ar-CO ₂ ⁺	0.26	PI	52
N ₂ -O ₂ ⁺	0.24	EQ	53
OCS-CS ₂ ⁺	0.25	PI	35
CS ₂ -S ₂ ⁺	0.99(0.95) ^b	EQ	36

^a The key is: TC, theoretical calculation; DS, differential scattering experiment; PI, photoionization of neutral cluster; EI, electron impact of neutral cluster; PD, photodissociation; EQ, equilibrium measurement; and SP, spectroscopy.

^b For the equilibrium measurements where we, rather than the authors, extrapolated the measured enthalpy change to 0 K the measured enthalpy change is given in brackets.

where T can be taken to be the middle of the temperature range studied. To be rigorous the measured enthalpy change should be extrapolated to 0 K,⁵⁴ which we have done for the data in Table II when the extrapolation was not performed by the authors.

For the rare gas dimers the agreement between dissociation energies measured using different techniques is satisfactory. However, for the molecular dimers the agreement between the photoionization and equilibrium measurements is rather poor in some cases. Lee and co-workers^{31,40,47} have suggested that for the rare gas dimers the large density of Rydberg states around the adiabatic ionization threshold compensates for the poor Franck–Condon factors. As noted by Stephan *et al.*⁴⁸ this may not be the case in molecular systems: the Rydberg states may predissociate instead of autoionize. Furthermore, in molecular systems rather more extensive geometry changes are involved. For example, $\text{N}_2\cdot\text{N}_2^+$ has C_{2v} symmetry⁵⁵ and $\text{N}_2\cdot\text{N}_2^+$ is probably linear.⁴⁹

It is evident from Table II that the number of asymmetric molecular systems for which dissociation energies have been measured is rather small. For $\text{Ar}\cdot\text{CO}_2^+$, $\text{N}_2\cdot\text{O}_2^+$, and $\text{OCS}\cdot\text{CS}_2^+$ the measured dissociation energies lie between 0.24 and 0.26 eV. The dissociation energy of $\text{Kr}\cdot\text{O}_2^+$ (~ 0.33 eV) is slightly larger. Compared with these values the dissociation energy for $\text{CS}_2\cdot\text{S}_2^+$ (0.99 eV) is surprisingly large and indicates that some fairly strong chemical bonding must arise in $\text{CS}_2\cdot\text{S}_2^+$.

The bonding in ion–molecule clusters is a topic which has received some attention in recent years. It is now generally appreciated that electrostatic forces alone cannot account for the binding energies and that substantial chemical bonding is involved even for the weakly bound clusters.^{49,52,53} The chemical bonding is expected to increase as I. P.(A) – I. P.(B) for $\text{A}\cdot\text{B}^+$ decreases.^{52,53} Thus, as is evident from Table II, the symmetric dimers are more strongly bound, in general, than the asymmetric clusters, and along a series such as $\text{Xe}\cdot\text{Xe}^+$, $\text{Xe}\cdot\text{Kr}^+$, $\text{Xe}\cdot\text{Ar}^+$, and $\text{Xe}\cdot\text{Ne}^+$ the dissociation energy decreases. A simple picture of the chemical bonding in these species can be obtained by considering the chemical bonding to arise from transfer of electron density from the highest occupied molecular orbital (HOMO) of the molecule to the lowest unoccupied molecular orbital (LUMO) of the ion. This simple picture has some success. For example, for $\text{N}_2\cdot\text{N}_2^+$, $\text{CO}\cdot\text{CO}^+$, $\text{NO}\cdot\text{NO}^+$, and $\text{O}_2\cdot\text{O}_2^+$ the first two members of this list are bound by around 1 eV, whereas the last two members are bound by around half this energy. Why should these clusters, which superficially appear similar, have such different dissociation energies? For $\text{N}_2\cdot\text{N}_2^+$ and $\text{CO}\cdot\text{CO}^+$, which are isoelectronic, the HOMO/LUMO interaction is σ/σ , as shown in Fig. 9, so it is easy to understand why these clusters are strongly bound and why $\text{N}_2\cdot\text{N}_2^+$ is predicted to be linear by *ab initio* theory. In contrast, for $\text{O}_2\cdot\text{O}_2^+$ and $\text{NO}\cdot\text{NO}^+$ the HOMO/LUMO interaction is π^*/π^* , as shown in Fig. 9, which will be a weaker interaction than σ/σ . For a π^*/π^* interaction a parallel structure would be expected to be stable. There is some experimental evidence that $\text{NO}\cdot\text{NO}^+$ has a *cis*-trapezoid structure²⁶ and semiempirical calculations for $\text{O}_2\cdot\text{O}_2^+$ predict that the *cis*-trapezoid structure is stable, although the *trans*

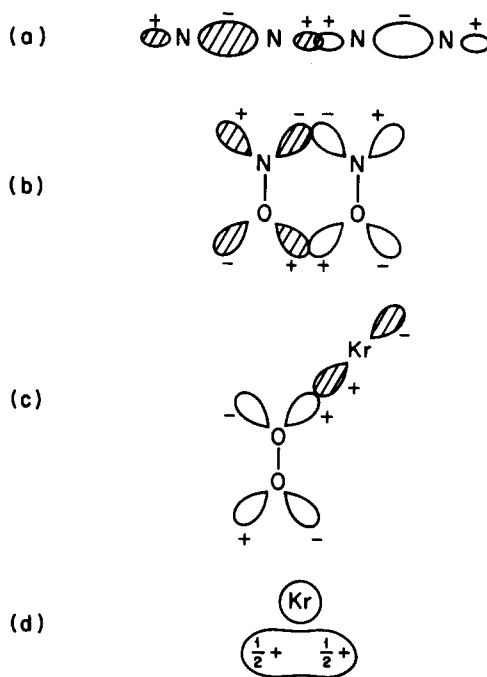


FIG. 9. Diagrams showing the interactions between the HOMO of the molecule (shaded) and the LUMO of the ion for (a) $\text{N}_2\cdot\text{N}_2^+$; (b) $\text{NO}\cdot\text{NO}^+$; and (c) $\text{Kr}\cdot\text{O}_2^+$; (d) shows the structure for $\text{Kr}\cdot\text{O}_2^+$ expected from simple electrostatic considerations.

structure is predicted to be slightly more stable.⁵⁶ For $\text{Kr}\cdot\text{O}_2^+$ the HOMO/LUMO interaction is p/π_g which will be weakly bonding in the bent configuration as shown in Fig. 9. Electrostatic forces will also make an important contribution to the bonding in weakly bound clusters such as $\text{Kr}\cdot\text{O}_2^+$. From a simple electrostatic point of view, putting $1/2+$ on each O atom, we would expect $\text{Kr}\cdot\text{O}_2^+$ to have C_{2v} symmetry with the Kr snuggled up between the two oxygen atoms as shown in Fig. 9. Thus, from consideration of the chemical bonding we expect a bent structure from $\text{Kr}\cdot\text{O}_2^+$ but from electrostatics a C_{2v} structure. Clearly the structure of $\text{Kr}\cdot\text{O}_2^+$ will be determined by a balancing of electrostatic and chemical forces. More will be said about this point later.

The values for the asymmetry parameter deduced from the simulations were $\beta_0 = 1.0$ – 1.2 for wavelengths ≥ 514 nm and $\beta_0 > 0.4$ for 575 nm. β_0 can have values in the range $+2 > \beta > -1$. Values of β outside the range $+0.5 > \beta > -0.25$ indicate that the lifetime of the excited state is much less than a rotational period.^{57,58} For values of β within this range the lifetime of the excited state may be larger than a rotational period. Thus, values of β_0 found for wavelengths ≥ 514 nm indicate that the excited state has a lifetime much shorter than a rotational period which suggests that photodissociation occurs by a direct transition to a repulsive surface. For a wavelength of 575 nm the interpretation of $\beta_0 > 0.4$ is ambiguous. However, we do not believe that this result indicates a lifetime longer than a rotational period. The low limit probably reflects the problems we had in analyzing these data. Values of $\beta > 0$ generally indicate that the transition dipole moment is orientated mainly in the direction of the interfragment axis of the cluster, while values of $\beta < 0$ generally indicate an orientation perpendicular to the interfragment axis. The values of β_0 for $\text{Kr}\cdot\text{O}_2^+$ suggest the transition dipole moment is orientated mainly paral-

lel to the interfragment axis in the cluster. Viewing the transition as a photon assisted charge transfer,¹ it is intuitively obvious that the transition dipole moment should be along the interfragment axis of the cluster.

It is clear from the product relative kinetic energy distributions (Figs. 3 and 4) that quite specific energy disposal occurs in the photodissociation of the $\text{Kr}\cdot\text{O}_2^+$ cluster. As is evident from the plot of the average kinetic energy against photon energy (Fig. 7), for wavelengths smaller than 514 nm, an increase in the photon energy does not result in a substantial increase in the product relative kinetic energy. Thus, the extra available energy must be channeled into internal excitation of the products. The features observed in the product relative kinetic energy distributions (Figs. 3 and 4) suggest that the extra energy appears mainly as O_2 vibrational excitation (with the possible exception of the UV data discussed below). Assuming the vibrational state assignments given in Fig. 4 are correct, for 514 nm the O_2 is produced mainly in the $v = 0$ state. For ground state $\text{Kr}\cdot\text{O}_2^+$ the $v = 1$ state is not accessible at this wavelength. However, the sharp feature at close to zero relative kinetic energy (Fig. 3) is probably due to O_2 in the $v = 1$ state from the photodissociation of internally excited $\text{Kr}\cdot\text{O}_2^+$. For a wavelength of 488 nm the $v = 1$ and $v = 0$ states of O_2 are accessible. The O_2 is produced mainly in the $v = 1$ state along with a significant population in the $v = 0$ state. Up to $v = 2$ is accessible for a wavelength of 458 nm. The product relative kinetic energy distribution indicates that the O_2 is probably mainly in the $v = 2$ state with a substantial component in the $v = 1$ state and possibly a small component in the $v = 0$ state. Unfortunately, it is not possible to derive accurate relative populations of the product vibrational states from the kinetic energy distributions because the features are not sufficiently resolved. However, an estimate of the product vibrational state distributions can be obtained by assuming that the components with the lowest kinetic energy in the 488 and 458 nm distributions have the same shape as the $v = 0$ peak in the 514 nm distribution. Thus, the relative populations of the vibrational states can be derived by subtracting the 514 nm $v = 0$ peak from the distributions. The results of this analysis are given in Table III.

The bond length in $\text{O}_2^+(X^2\Pi_g)$ is shorter than in $\text{O}_2(X^3\Sigma^-)$. As a result, on ionization of $\text{O}_2(X^3\Sigma^-)$ the internuclear separation decreases and $\text{O}_2^+(X^2\Pi_g)$ is vibrationally excited. This is clear from the photoelectron spectrum of O_2 .⁵⁹ Analogous bond length changes occur in the photodissociation of $\text{Kr}\cdot\text{O}_2^+$. Here the transition is from a $\text{Kr}\cdot\text{O}_2^+$ state to a $\text{Kr}^+\cdot\text{O}_2$ state so the O–O internuclear separation increases. The Franck–Condon factors for the $\text{O}_2(X^3\Sigma^-, v')$

$\leftarrow\text{O}_2^+(X^2\Pi_g, v'' = 0)$ transition are 0.188, 0.365, 0.290, 0.123, and 0.03 for $v' = 0$ to $v' = 4$, respectively.⁶⁰ Thus the vibrational excitation of the O_2 observed in the photodissociation of $\text{Kr}\cdot\text{O}_2^+$ in the wavelength range 514–458 nm could be accounted for in terms of changes in the O–O internuclear separation on going from the $\text{Kr}\cdot\text{O}_2^+$ state to the $\text{Kr}^+\cdot\text{O}_2$ state. The Franck–Condon factors slightly favor production of O_2 in the $v = 1$ state. From the 458 nm kinetic energy distribution the O_2 appears to be produced preferentially in the $v = 2$ state. It is not clear that very much significance should be attached to this observation because the Franck–Condon factors are for free O_2/O_2^+ . However, this result may indicate a trend for preferential production of O_2 in the highest accessible vibrational state as the photon energy is raised. The results discussed above indicate that the potential surface is fairly flat along the Kr^+-O_2 coordinates in the region sampled. Thus, raising the photon energy results in going up the O–O stretch coordinate vibrational ladder, which leads to high product vibrational excitation, rather than up a repulsive Kr^+-O_2 coordinate which would lead to high product relative kinetic energies.

In Fig. 4 the features in the distributions which occur at approximately the same value of $h\nu - \Delta I. P. - KE$ arise from O_2 formed in the same vibrational state. We noted in the results section that as the photon energy is raised, there is a tendency for the features corresponding to the formation of O_2 in a specific vibrational state to become broader and shift to slightly higher values of $h\nu - \Delta I. P. - KE$. This corresponds to a shift to smaller values of relative kinetic energy and almost certainly arises mainly from rotational excitation of the product O_2 . We will illustrate this result using the 458 nm kinetic energy distribution (Fig. 3). The peak in this distribution at ~ 0.05 eV was assigned to O_2 ($v = 2$) and the peak at ~ 0.2 eV was assigned to O_2 ($v = 1$). A scale in the middle of this distribution shows the energy separation between the $v = 1$ and $v = 2$ vibrational levels of O_2 . This energy separation does not exactly match the separation between the two peaks. Assuming that the vibrational energy is deposited in the O–O stretch coordinate by the optical transition, then for O_2 ($v = 1$) there is more energy available as the products separate than for O_2 ($v = 2$). All this energy may not appear as product kinetic energy. Some of it can be channeled into rotational excitation as the products separate on the repulsive surface. As shown in Fig. 3 an estimate of the partitioning of this extra energy between rotational excitation of the O_2 and relative kinetic energy can be obtained from the energy separation between the two peaks. This estimate will be an upper limit on the rotational excitation because the peaks corresponding to formation of O_2 in different vibrational states overlap. The overlap of the peaks will result in a reduction in the apparent separation between the maxima. To account for this effect we need to deconvolute the individual components. Assuming that the shape of the lower energy component in the distributions is the same as the shape of the 514 nm $v = 0$ component, an approximate deconvolution can be performed and the true energy separation between the maxima determined. In this manner we deduce that around 20% of the extra available energy is channeled into rotational excitation of the O_2 . This result

TABLE III. Estimate of product O_2 vibrational state distribution for photodissociation of KrO_2^+ at the indicated wavelengths (see the text).

Vibrational state	Wavelength (nm)		
	514	488	458
$v = 0$	0.75	0.15	0.2
$v = 1$	0.25	0.85	
$v = 2$	0.8

can be compared with the predictions of a simple impulsive model⁶¹ which gives the rotational excitation of the products as

$$E_{\text{ROT}} = \sin^2 \alpha \left(1 - \frac{\mu_{\text{BC}}}{\mu_{\text{F}}} \right) E_{\text{AV}} \quad (14)$$

for a loose O-O bond and

$$E_{\text{ROT}} = \sin^2 \alpha \left[\left(1 - \frac{\mu_{\text{BC}}}{\mu_{\text{F}}} \right)^{-1} - \cos^2 \alpha \right]^{-1} E_{\text{AV}} \quad (15)$$

for a stiff O-O bond. In these equations μ_{F} is the reduced mass of the products, μ_{BC} is the reduced mass of the atoms at the end of the breaking bond (Kr and O) and $180 - \alpha$ is the O-O-Kr bond angle. Using these equations we can extract a bond angle for Kr-O₂⁺ from our data on the product rotational excitation. We obtain a value of 135° for a loose O-O bond and 143° for a stiff O-O bond. Since the O-O bond is neither infinitely stiff or infinitely loose these results imply a bond angle for Kr-O₂⁺ of around 139°. A bent geometry for Kr-O₂⁺ is in agreement with the HOMO/LUMO model discussed above. Only low rotational excitation of the O₂ would be expected for dissociation from the C_{2v} structure derived from simple electrostatics.

For photodissociation with the UV lines the average product relative kinetic energy was approximately the same as observed for photodissociation in the visible region of the spectrum. Thus, the extra energy available in the UV photon must appear as internal excitation of the products. As noted above the higher energy Kr⁺(²P_{1/2}) spin state and the first excited O₂(¹Δ_g) state are both accessible with the UV lines. We have shown on the UV product kinetic energy distribution (Fig. 6) separate scales showing the extent of product vibrational excitation assuming that Kr⁺ is formed in the ²P_{3/2} state and in the ²P_{1/2} state. If there is only low product rotational excitation, which we would expect from the preceding discussion, then for the Kr⁺ to be formed in the ²P_{3/2} state the O₂ must be mainly in $v = 6$, and if Kr⁺(²P_{1/2}) is formed O₂ will probably be mainly in $v = 2$. We believe that the product is unlikely to be Kr⁺(²P_{3/2}) for the following reason: If the product were Kr⁺(²P_{3/2}) then the internal excitation required to produce O₂ ($v = 6$) with such low product relative kinetic energy would have to be deposited into the O-O stretch coordinate by the optical transition. However, the Franck-Condon factor⁶⁰ for a transition into O₂ ($v = 6$) is extremely small. Thus we believe that one of the products must be electronically excited [i.e., either Kr⁺(²P_{1/2}) or O₂(¹Δ_g)]. These electronically excited products will be generated by a transition to a different potential surface from the ground state products formed in the visible region of the spectrum. If the electronically excited product is Kr⁺(²P_{1/2}) then the general features of the UV kinetic energy distribution are consistent with the idea discussed above that the product O₂ is produced preferentially in the highest accessible vibrational state. This suggests that the ²P_{1/2} surface is similar to the ²P_{3/2} surface and is fairly flat along the Kr⁺-O₂ coordinates in the region sampled.

Charge transfer from Kr⁺ + O₂ occurs at around 8% of the collision rate for the ²P_{3/2} state of Kr⁺ and at <0.2% of the collision rate for the ²P_{1/2} state⁴ at thermal energies. We observed no O₂⁺ product from the photodissociation of

Kr-O₂⁺. This result indicates that the charge transfer reaction and photodissociation of Kr-O₂⁺ either involve different potential surfaces or that the two processes occur on different regions of the same surface. In Fig. 10 we have shown some schematic potential curves for the doublet states of [Kr-O₂]⁺ in C_s(C_{2v}) symmetry. We have used a molecular orbital description of the states (cf. Ref. 5) that is appropriate for both the O₂⁺ + Kr states and for the Kr⁺ + O₂ states at small internuclear separation. The angular distributions indicated that the transition dipole moment is mainly parallel to the interfragment axis. Thus with C_s symmetry the allowed optical transitions are A' ↔ A' and A'' ↔ A''. The arrows in Fig. 10 show the allowed optical transitions. Transitions are allowed between the ²A''(²A₂) ground state and ²A'' states which correlate to both the spin orbit spin states of Kr⁺. The transition to the lower ²A'' state is shown going into the $v = 1$ state of the O-O stretch. As noted above, the O-O internuclear separation will be different in these two states and the Franck-Condon factors will favor production of O₂ in the $v = 1$ state. The middle ²A'' surface is drawn fairly flat along the Kr⁺-O₂ coordinate and it is easy to see how on raising the photon energy the transition goes up the O-O coordinate stretch rather than up a repulsive Kr⁺-O₂ coordinate.

The charge transfer reaction naturally arises from a transition from a Kr⁺ + O₂ surface to a Kr + O₂⁺ surface. We show in Fig. 10 a possible intersection between the ²A'(²A₁) surface and the ²A'(²B₂) surface which could give rise to the charge transfer reaction. Note that this intersection involves surfaces which are not involved in the photodissociation which accounts for why we were unable to detect O₂⁺ product in the photodissociation. Furthermore, the intersection occurs for a surface which arises from the Kr⁺(²P_{3/2}) spin state which accounts for why charge transfer is much faster for this state. The crossing between the upper ²A' state and the lower ²A' state becomes allowed in C_{2v} symmetry and this conical intersection acts like a funnel for trajectories to cross from the upper ²A' state to the lower ²A' state. If the reactants begin with equal probability on each potential sur-

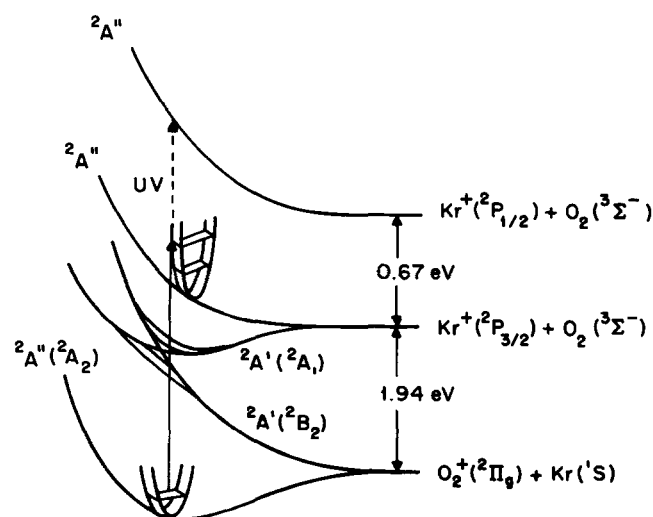


FIG. 10. Schematic potential curves for the [Kr-O₂]⁺ system in C_s(C_{2v}) symmetry. The arrows show allowed optical transitions for the transition dipole moment along the interfragment axis in the cluster.

face (including the quartet states) and if no transitions occur between the surfaces then only 1/6 of the $\text{Kr}^+(^2P_{3/2}) + \text{O}_2(^3\Sigma^-)$ collisions will end up on the A' surface at small r (see Ref. 5). Thus the probability of crossing from the $^2A'(^2A_1)$ surface to the $^2A'(^2B_2)$ surface could be fairly large as the measured rate is 8% of the collision rate. Jones *et al.*⁵ found that the rate constant decreased as the collision energy is raised. This can readily be understood in terms of the lifetimes of the loosely bound complex formed on the $^2A'(^2A_1)$ surface: the lifetime will be shorter for higher energy collision leading to a reduction in the probability of crossing over to the $^2B_2(A')$ surface. Marx *et al.*⁶ found that in the charge transfer reaction around 60% of the available energy appears as relative kinetic energy of the products which corresponds to production of O_2^+ in the $v = 3-4$ states. We believe that the specific energy disposal observed in the charge transfer reaction can be rationalized in terms of the properties of the intersection between the $^2A'(^2A_1)$ and $^2A'(^2B_2)$ surfaces. For a transition to occur between these surfaces it is necessary for the $\text{Kr}^+\cdot\text{O}_2$ to attain close to C_{2v} symmetry. Dissociation in a C_{2v} geometry on the repulsive part of the $^2A'(^2B_2)$ surface would favor only low rotational excitation of the products. To understand the product vibrational excitation it is necessary to consider the behavior of the O-O coordinate at the intersection. Bond length changes occur on going from O_2 to O_2^+ . From Franck-Condon factors the O_2^+ would be expected to be generated preferentially in the $v = 1$ and $v = 2$ states.⁶⁰ The additional vibrational excitation observed in the charge transfer reaction can probably be ascribed to distortion of the O-O potential in the region of the intersection by the Kr atom.

V. CONCLUSIONS

Our main conclusions are summarized below:

(1) Photodissociation of $\text{Kr}\cdot\text{O}_2^+$ in the visible and UV regions of the spectrum occurs by charge transfer transitions from a $\text{Kr}\cdot\text{O}_2^+$ state to $\text{Kr}^+\cdot\text{O}_2$ states. The only observed ionic product was Kr^+ which is consistent with the idea that charge transfer between Kr^+ and O_2 and the photodissociation process occur on different potential surfaces.

(2) In the visible region of the spectrum the products are $\text{Kr}^+(^2P_{3/2}) + \text{O}_2(^3\Sigma^-)$. In the UV one of the products is probably electronically excited [i.e., $\text{Kr}^+(^2P_{1/2})$ or $\text{O}_2(^1\Delta_g)$].

(3) The dissociation energy of the $\text{Kr}\cdot\text{O}_2^+$ cluster is $D_0^\circ(\text{Kr}\cdot\text{O}_2^+) \sim 0.33$ eV.

(4) The product angular distributions indicate that the lifetimes of the excited states involved in the photodissociation process are less than a rotational period, which is consistent with these states being repulsive. The transition dipole moment is orientated mainly parallel to the interfragment axis of the cluster.

(5) Resolved features in the product relative kinetic energy distributions were assigned to production of O_2 in specific vibrational states. The data indicate that most of the available energy is partitioned into vibrational excitation with the O_2 produced preferentially in the highest accessible vibrational state. This energy is deposited into the O-O stretch coordinate mainly by the optical transition. The maximum observed vibrational excitation was slightly above that predicted from Franck-Condon factors for free $\text{O}_2/$

O_2^+ . These results indicate that the potential surface is relatively flat along the Kr^+-O_2 coordinates in the region sampled.

(6) Around 20% of the repulsive energy between the fragments is channeled into rotational excitation of the O_2 . Comparison with the predictions of simple impulsive models suggests that $\text{Kr}\cdot\text{O}_2^+$ is bent with a Kr-O-O bond angle of around 139° . A bent structure for $\text{Kr}\cdot\text{O}_2^+$ is in agreement with a simple HOMO/LUMO model for the chemical bonding in $\text{Kr}\cdot\text{O}_2^+$.

(7) A fairly complete qualitative picture of the $[\text{Kr}\cdot\text{O}_2]^+$ potential surfaces can be obtained by considering the photodissociation results in conjunction with literature data on the charge transfer reaction between Kr^+ and O_2 .

ACKNOWLEDGMENTS

We gratefully acknowledge the support of the Air Force Office of Scientific Research under grant AFOSR-82-0035 and the National Science Foundation under grant CHE80-20464. One of us (L. M.) also acknowledges the Swiss National Science Foundation for a fellowship. We thank Professor Malcolm Nicol for suggesting that $\text{O}_2(^1\Delta_g)$ might be a product in the UV photodissociation process.

¹D. A. Copeland and C. L. Tang, *J. Chem. Phys.* **65**, 3161 (1976).

²L. F. Errea, L. Mendez, and E. Riera, *J. Chem. Phys.* **79**, 4221 (1983).

³H. M. Rosenstock, K. Draxl, B. W. Steiner, and J. T. Herron, *J. Phys. Chem. Ref. Data* **6**, Suppl. No. 1 (1977).

⁴N. G. Adams, D. Smith, and E. Alge, *J. Phys. B* **13**, 3235 (1980).

⁵T. T. C. Jones, K. Birkinshaw, J. D. C. Jones, and N. D. Twiddy, *J. Phys. B* **15**, 2439 (1982).

⁶R. Marx, G. Mauclaire, T. R. Govers, M. Gerard-Ain, and R. Derai, *J. Chim. Phys.* **76**, 1077 (1979).

⁷M. F. Jarrold, A. J. Illies, and M. T. Bowers, *J. Chem. Phys.* **79**, 6086 (1983).

⁸M. F. Jarrold, A. J. Illies, and M. T. Bowers, *J. Chem. Phys.* **81**, 214 (1984).

⁹M. F. Guest, A. Ding, J. Karlan, J. Weise, and I. H. Hillier, *Mol. Phys.* **38**, 1427 (1979).

¹⁰K. P. Huber and G. Herzberg, *Constants of Diatomic Molecules* (Van Nostrand, New York, 1979).

¹¹Treating the vibrations as quantized and the rotations classically the probability of an internal energy E is $P_{v+r}(E) = \sum_v P_v(E_v) \cdot P_R(E - E_v)$, where $P_v(E_v)$ is the probability of vibrational energy E_v given by $e^{-E_v/kT}$ and $P_R(E - E_v)$ is the probability of rotational energy $E - E_v$ which is given by $e^{-(E - E_v)/kT}$ for a linear molecule and $(E - E_v)^{1/2} e^{-(E - E_v)/kT}$ for a nonlinear molecule.

¹²The required input data for Eq. (8) are the vibrational frequencies and whether the cluster is linear or nonlinear. The distributions shown in Fig. 3(a) were calculated assuming a nonlinear geometry and using the frequencies: 1600, 100, and 50 cm^{-1} . These are reasonable values and trial calculations indicated that the calculated distributions were not very sensitive to the choice of input data.

¹³R. N. Zare, *Mol. Photochem.* **4**, 1 (1972); G. E. Busch and K. R. Wilson, *J. Chem. Phys.* **56**, 3638 (1972).

¹⁴ $P(\alpha; E_r, T)$ depends on whether the cluster is linear or nonlinear. We assumed a nonlinear structure and used a temperature of 100 K in the simulation. Although we have noted the internal energy distribution has a high energy tail it is reasonable to use a temperature of 100 K to characterize the rotational energy distribution because the rotational distribution is expected to be equilibrated more quickly than the vibrational distribution.

¹⁵B. Liu, *Phys. Rev. Lett.* **27**, 1251 (1971).

¹⁶R. E. Olson and C. R. Mueller, *J. Chem. Phys.* **46**, 3810 (1967).

¹⁷H. P. Weise, H. U. Mittmann, A. Ding, and A. Henglein, *Z. Naturforsch. Teil A* **26**, 1122 (1971).

¹⁸D. J. Trevor, Ph. D. thesis, University of California, Berkeley, 1980.

¹⁹H. U. Mittmann and H. P. Weise, *Z. Naturforsch. Teil A* **29**, 400 (1974).

²⁰J. T. Moseley, R. P. Saxon, B. A. Huber, P. C. Cosby, R. Abouaf, and M.

- Tadjeddine, *J. Phys. Chem.* **67**, 1659 (1977).
- ²¹P. M. Dehmer and S. T. Pratt, *J. Chem. Phys.* **76**, 843 (1982).
- ²²R. Abouaf, B. A. Huber, P. C. Cosby, R. P. Saxon, and J. T. Moseley, *J. Chem. Phys.* **68**, 2406 (1978).
- ²³S. T. Pratt and P. M. Dehmer, *Chem. Phys. Lett.* **87**, 533 (1982).
- ²⁴C. Y. Ng, D. J. Trevor, B. H. Mahan, and Y. T. Lee, *J. Chem. Phys.* **66**, 446 (1977).
- ²⁵C. Y. Ng, D. J. Trevor, B. H. Mahan, and Y. T. Lee, *J. Chem. Phys.* **65**, 4327 (1976).
- ²⁶S. H. Linn, Y. Ono, and C. Y. Ng, *J. Chem. Phys.* **74**, 3343 (1981).
- ²⁷J. D. Payzant and P. Kebarle, *J. Chem. Phys.* **53**, 4723 (1970); the experimental enthalpy change (0.989 eV) at $T \sim 790$ K was extrapolated to 0 K assuming a linear structure for N₂·N₂⁺ as predicted by *ab initio* theory (Ref. 49) and using the values 250 (1) and 100 cm⁻¹ (4) for the low frequency vibrational modes of the cluster.
- ²⁸D. C. Conway and J. S. Janik, *J. Chem. Phys.* **53**, 1859 (1970); the measured enthalpy change was extrapolated to 0 K by the authors.
- ²⁹S. H. Linn, Y. Ono, and C. Y. Ng, *J. Chem. Phys.* **74**, 3348 (1981).
- ³⁰C. Y. Ng, P. W. Tiedemann, B. H. Mahan, and Y. T. Lee, *J. Chem. Phys.* **66**, 3985 (1977).
- ³¹P. W. Tiedemann, S. L. Anderson, S. T. Ceyer, T. Hirooka, C. Y. Ng, B. H. Mahan, and Y. T. Lee, *J. Chem. Phys.* **71**, 605 (1979).
- ³²S. H. Linn and C. Y. Ng, *J. Chem. Phys.* **75**, 4921 (1981).
- ³³J. V. Headley, R. S. Mason, and K. R. Jennings, *J. Chem. Soc. Faraday Trans. 1* **78**, 933 (1982); also see P. A. M. van Koppen, P. R. Kemper, A. J. Illies, and M. T. Bowers, *Int. J. Mass Spectrom. Ion Process.* **54**, 263 (1983); the experimental enthalpy change, 0.685 eV, at $T \sim 510$ K was extrapolated to 0 K assuming a D_{2h} structure for CO₂·CO₂⁺ with a C–C distance of 2 Å and using the values 200 (1), 120 (1), and 50 cm⁻¹ (2) for the low frequency vibrational modes. If one of the vibrational modes is replaced by an internal rotor the 0 K dissociation energy becomes 0.69 eV.
- ³⁴G. G. Jones and J. W. Taylor, *J. Chem. Phys.* **68**, 1768 (1978).
- ³⁵Y. Ono, E. A. Osuch, and C. Y. Ng, *J. Chem. Phys.* **74**, 1645 (1981).
- ³⁶M. Meot-Ner and F. H. Field, *J. Chem. Phys.* **66**, 4527 (1977). For CS₂·CS₂⁺ the experimental enthalpy change (0.95 eV) at $T \sim 620$ K was extrapolated to 0 K assuming a D_{2h} structure for CS₂·CS₂⁺ with a C–C distance of 3 Å and using the values 180 (1), 90 (1), and 45 cm⁻¹ (2) for the low frequency vibrational modes. For CS₂·S₂⁺ the experimental enthalpy change (0.95 eV) at $T \sim 620$ K was extrapolated to 0 K assuming a C_{2v} structure with a CS₂–S₂⁺ distance of 3 Å and using the values 120 (1), 60 (1), and 30 cm⁻¹ (2) for the low frequency vibrational modes.
- ³⁷Y. Ono, S. H. Linn, H. F. Prest, M. E. Gress, and C. Y. Ng, *J. Chem. Phys.* **73**, 2523 (1980).
- ³⁸W. M. Trott, N. C. Blais, and E. A. Walters, *J. Chem. Phys.* **71**, 1692 (1979).
- ³⁹J. Erickson and C. Y. Ng, *J. Chem. Phys.* **75**, 1650 (1981).
- ⁴⁰S. T. Ceyer, P. W. Tiedemann, B. H. Mahan, and Y. T. Lee, *J. Chem. Phys.* **70**, 14 (1979).
- ⁴¹S. T. Ceyer, P. W. Tiedemann, C. Y. Ng, B. H. Mahan, and Y. T. Lee, *J. Chem. Phys.* **70**, 2138 (1979).
- ⁴²I. Dabrowski and G. Herzberg, *J. Mol. Spectrosc.* **73**, 183 (1978).
- ⁴³S. T. Pratt and P. M. Dehmer, *J. Chem. Phys.* **76**, 3433 (1982).
- ⁴⁴I. Dabrowski, G. Herzberg, and K. Yoshino, *J. Mol. Spectrosc.* **89**, 491 (1981).
- ⁴⁵P. M. Dehmer and S. T. Pratt, *J. Chem. Phys.* **77**, 4804 (1982).
- ⁴⁶C. Y. Ng, P. W. Tiedemann, B. H. Mahan, and Y. T. Lee, *J. Chem. Phys.* **66**, 5737 (1977).
- ⁴⁷C. Y. Ng, D. J. Trevor, P. W. Tiedemann, S. T. Ceyer, P. L. Kronebusch, B. H. Mahan, and Y. T. Lee, *J. Chem. Phys.* **67**, 4235 (1977).
- ⁴⁸K. Stephan, J. H. Futrell, K. I. Peterson, A. W. Castleman, and T. D. Mark, *J. Chem. Phys.* **77**, 2408 (1982).
- ⁴⁹S. C. de Castro, H. F. Schaefer, and R. M. Pitzer, *J. Chem. Phys.* **74**, 550 (1981).
- ⁵⁰J.-H. Yang and D. C. Conway, *J. Chem. Phys.* **40**, 1729 (1964); the measured enthalpy change was extrapolated to 0 K by the authors.
- ⁵¹S. L. Anderson, T. Hirooka, P. W. Tiedemann, B. H. Mahan, and Y. T. Lee, *J. Chem. Phys.* **73**, 4779 (1980).
- ⁵²S. T. Pratt and P. M. Dehmer, *J. Chem. Phys.* **78**, 6336 (1983).
- ⁵³G. S. Janik and D. C. Conway, *J. Phys. Chem.* **71**, 823 (1967); the measured enthalpy change was extrapolated to 0 K by the authors.
- ⁵⁴Assuming an ideal gas model, neglecting electronic contributions and cancelling the high frequency modes in A⁺, A, and A·A⁺ the relationship between ΔH_T° and ΔH_0° is
- $$\Delta H_0^\circ = \Delta H_T^\circ + \frac{1}{2}(5 + R)kT - N \sum_{v_i} h\nu_i / \left(e^{\frac{h\nu_i}{kT}} - 1 \right),$$
- where R is the number of rotational degrees of freedom lost in the association reaction and the last term is the contribution from the low frequency vibrational modes formed in the association reaction. As illustrated in Refs. 28, 50, and 53 the experimentally determined ΔS can be used as a guide to estimate the low frequency vibrational modes and the extrapolation to 0 K can be accomplished without introducing significant uncertainty.
- ⁵⁵B. L. Blaney and G. E. Ewing, *Annu. Rev. Phys. Chem.* **27**, 553 (1976).
- ⁵⁶D. C. Conway, *J. Chem. Phys.* **50**, 3864 (1969).
- ⁵⁷C. Jonah, *J. Chem. Phys.* **55**, 1915 (1971).
- ⁵⁸S. Yang and R. Bersohn, *J. Chem. Phys.* **61**, 4400 (1974).
- ⁵⁹J. H. D. Eland, *Photoelectron Spectroscopy* (Butterworths, London, 1974).
- ⁶⁰P. H. Krupenie, *J. Phys. Chem. Ref. Data* **1**, 423 (1972).
- ⁶¹G. E. Busch and K. R. Wilson, *J. Chem. Phys.* **56**, 3626 (1972).